Numerical modeling of the power losses in geared transmissions: Windage, churning and cavitation simulations with a new integrated approach that drastically reduces the computational effort

Franco Concli [a,n,1], Carlo Gorla [b]

[a] Faculty of Science and Technology, Free University of Bolzano, piazza Università 5, 39100, Bolzano (BZ), Italy
[b] Department of Mechanical Engineering, Politecnico di Milano, via La Masa 1, 20157, Milano (MI), Italy

Energy savings and efficient design are the new global trends. Gears are the main components in many applications like vehicle transmissions, industrial gearboxes etc. and although they are already highly efficient, there is still margin for improvement. Depending on the sector of application, energy saving produces also additional benefits such as a reduction of the pollutant emission in the automotive branch or an increased reliability/power density in compact applications like the precision planetary gearboxes.

To perform efficiency improvements it is important to be able to compare different design solutions. A lot of research was made on gears but still today accurate power loss models are not available. Recently, the adoption of numerical techniques has enabled the overcoming of this problem but with the drawback of very long computational times.

Considering the importance of such topic for gearbox manufacturers, the authors have developed a specific power loss calculation-tool that enables a good prediction accuracy with reasonable computa-tional efforts. The model was validated with experimental tests performed by FZG showing good agreement.

Keywords: Gears, CFD, Churning, Windage, Cavitation, Mesh-handling

1. Introduction

In the last years, the reduction of the power dissipation is becoming more and more a main issue. Gearbox efficiency is therefore important considering that geared solutions are normally part of more complex systems. Beside the pure energy saving aspects, solutions that are more efficient have lower operating temperatures and, consequently, a higher reliability or the capability to increase the power density without the failure of the lubricant.

Depending on the operating conditions and the geometrical configuration of the gearbox, the share among the different sources of loss can vary significantly. However, while the load dependent power losses were deeply studied in the past and the residual margins of improvement are low unless very unusual tooth proportions are considered, the load independent power losses are still difficult to predict and reduce consequently. The first works on this topic were carried out by Daily et al. [1], by Mann et al. [2] and by Soo et al. [3] considering a single gear, disk, or bladed rotor immersed in oil respectively. The main goal of these studies was to extrapolate from the experiments dimensionless churning coefficients. Specific studies on the churning power losses comprise those of Terekhov [4], Lauster et al. [5] and more recently Boness [6] and Changenet et al. [7]. Terekhov developed empirical relations for different gear geometries partially immerged into an oil bath. Walter [8] subsequently extended the original equations proposed by Terekhov. Starting from these results, Mauz [9] studied the load independent losses of gearboxes. In his work, Mauz adopted a test bench with a housing made of Plexiglas so to be able to observe the fluxes of lubricant inside the gearbox. The model proposed by Mauz is still the most complete model available in literature even if it is not so accurate and its range of application limited. Recently, some authors have applied numerical techniques for the study of the power loss mechanism in gears [10,11].

Different contributions have already shown the effectiveness of the CFD approach for such purposes. In the past, also the authors perform several studies [12–20] in that way. The main limitations

Article history:
Received 14 March 2016
Received in revised form
28 June 2016
Accepted 30 June 2016
Available online 5 July 2016

* Corresponding author.
[1] [Contract Professor]

Published Journal Article available at: http://dx.doi.org/10.1016/j.triboint.2016.06.046

Nomenclature

$C^+; C^-$	empirical constants [s^{-1}]
Co	Courant number []
$\boldsymbol{F}$	external forces [N]
$\boldsymbol{g}$	gravity [ms^{-2}]
$\dot{m}$	mass transfer [kg m^3]
$\dot{m}^+$	vaporization [kg m^3]
$\dot{m}^-$	condensation [kg m^3]
p	pressure [Pa]
$\bar{p}$	filtered pressure [Pa]
p_v	vaporization pressure [Pa]
P_{LG0}	Load indep. gear power loss [W]
t_∞, U_∞	Kunz coefficients [ms^{-1}][s]
u	velocity component [ms^{-1}]
$\boldsymbol{v}$	velocity [ms^{-1}]
τ	Reynolds term [Pa]
$\boldsymbol{v}_C$	artificial velocity [ms^{-1}]
x	Cartesian coordinate [m]
α	volume fraction []
μ	viscosity [kg ms^{-1}]
ρ	density [kg m^3]

Sub indexes

i	direction index
j	direction index
l	liquid
v	vapor

to the wide diffusion of such approach are the computational effort, the complexity of setting up a model with a general-purpose software and the costs for the licenses. In this scenario, the authors started studying a simplified configuration [21] with the open-source code OpenFOAM® [22]. The authors have also developed [23] a new integrated approach for the prediction of the windage power losses of gears based on an effective mesh-handling algorithm that has shown a drastic reduction of the CFD simulation times. The same approach was tested for the simulation of the churning and the windage power loss including cavitation. The numerical results were compared with previously available experimental data [24].

2. Load independent power loss

The power losses in geared transmissions can be attributable to gears, bearings, seals and, for more complex transmissions in which they are present, to clutches or synchronizers. Gear and bearing losses can be furtherly subdivided into load dependent and load independent ones. The load independent power losses of gears are classifiable into three main groups: windage, squeezing/pocketing and churning losses. Adopting the specific terminology of fluid mechanics, windage occurs when the gears interact with one single fluid as big gears that are lubricated with a small layer of grease and interact (in terms of power dissipation) either only with the air or, when the housing is completely filled, with lubricant. On the other side, when the splashing phenomenon involves two phases like in the most widely diffused oil-bath lubrication configurations, the proper term is churning. In both cases additional effects of squeezing/pocketing are present, related to the varying volume of the gap between the mating teeth that cause pressure gradients and additional axial flows, even if they are generally of a lower order of magnitude.

As for the gears, the load independent power losses generated by the bearings are related to the interaction with the lubricant.

The shear among the losses can vary significantly depending on the geometrical configuration of the system. Strasser [25] states that a typical shear of the losses is: 20% attributable to bearings, 70% to gears and 10% to seals. Strasser furtherly indicates that for a parallel axis gearbox under deep lubrication, the gear losses (70% of the total) can be indicatively attributed for the 70% to the meshing ($\approx$ 50% of the total) and 30% to the interaction with the lubricant ($\approx$ 20% the total). Even if this is just an indication, it points out the importance to be able to predict the load independent gear losses. This becomes also more important in planetary gearboxes [18].

3. Numerical approach

The methodology presented in this paper relies on the solution of two balance equations that mathematically represent the conservation laws of mass and momentum

$$\frac{\partial \rho}{\partial t} + \nabla \bullet (\rho \boldsymbol{v}) = 0 \tag{1}$$

$$\frac{\partial (\rho \boldsymbol{v})}{\partial t} + \nabla \bullet (\rho \boldsymbol{v}\boldsymbol{v}) = -\nabla p + \nabla \bullet \left[\mu \left(\nabla \boldsymbol{v} + \nabla \boldsymbol{v}^T \right) \right] + \rho \boldsymbol{g} + \boldsymbol{F} \tag{2}$$

in which ρ is the density, $\boldsymbol{v}$ is the velocity vector, μ the viscosity, $\boldsymbol{g}$ is the gravity vector and $\boldsymbol{F}$ represents the external forces. These basic equations describe the behavior of a transient incompressible flow.

The solution of the system of equation can be achieved only by means of numerical techniques, in this case based on a PIMPLE (merged PISO-SIMPLE) algorithm [15].

The SIMPLE algorithm is developed for steady-state conditions in order to reach the convergence in a very fast manner. This approach is very effective but does not contain temporal information. To provide a stable simulation a relaxation factor can be introduced. In the other side, the PISO algorithm, developed for transient simulations, is time conservative. The drawback is that, in order to ensure the convergence, the time step should be reduced significantly and the simulation time suffers. The PIMPLE algorithm takes the advantages of both methods. It performs all the iterations in SIMPLE mode (with relaxation) to ensure convergence also for big time steps and performs an additional final iteration without relaxation in PISO mode to ensure time consistency.

This basic set of equation can be applied only to the particular condition in which only one fluid is present inside the gearbox (windage). As presented in the next paragraphs, also this statement is not always valid. In the specific case in which a liquid (not a gas) fluid completely fills the gearbox at steady state condition (oil-windage), the solution of Eqs. (1) and (2) provides acceptable results only as far as cavitation does not takes place. Considering that lubricants can only stand very small negative pressures as shown by Jakobsson [26], a cavitation model should be added to the system of equations. In such condition, the momentum equation is solved considering the properties of the phases-mixture that are calculated as a weighted average of the properties of the two different phases of the fluid. Therefore density and viscosity of the mixture results in

$$\rho = \rho_v \bullet \alpha + \rho_l \bullet (1-\alpha); \mu = \mu_v \bullet \alpha + \mu_l \bullet (1-\alpha) \tag{3}$$

in which the subscripts v and l stand for vapor and liquid respectively.

The scalar quantity called volume fraction α is, in turn, calculated for each cell as

$$\frac{\partial}{\partial t}\alpha + \frac{\partial}{\partial x_i}(\alpha u_i) = 0 \tag{4}$$

A relatively recent development uses a compressive scheme for the discretization of the vapor volume fraction α. In this approach, an artificial supplementary velocity field $\boldsymbol{v}_C$ is defined in the vicinity of the interface in such a way that the local flow steepens the gradient of the volume fraction function and the interface resolution is improved. A number of different approaches to define the compressive velocity field are reported in literature, e.g. ClC-SAM (Compressive Interface Capturing Scheme for Arbitrary Meshes) as described by Ubbink [27] and the currently used multi-dimensional universal limiter with explicit solution [28], which limits the flux of the variables to guarantee a bounded solution.

Furthermore, a source term that should mimic the phase change rate should be added to the right hand side of the volume-fraction continuity Eq. (1) that becomes

$$\frac{\partial \alpha}{\partial t} + \nabla \bullet (\alpha \boldsymbol{v}) + \nabla \bullet \left(\boldsymbol{v}_C \alpha (1-\alpha)\right) = \frac{\dot{m}}{\rho_v} \tag{5}$$

This can be estimated with a phase-change model. In this study, the model proposed by Kunz [29] was implemented. The mass transfer is based on different strategies for vaporization and condensation. The vaporization, $\dot{m}^+$, is modeled to be proportional to the amount by which the pressure is below the vapor pressure and the amount of liquid present, while the condensation, $\dot{m}^-$, is modeled using a third order polynomial function of the vapor volume fraction

$$\dot{m}^+ = C^+ \rho_v (1-\alpha) \frac{\min\left[0,\ \bar{p} - p_v\right]}{1/2 \rho_l U_\infty^2 t_\infty} \tag{6}$$

$$\dot{m}^- = \frac{C^- \rho_v \alpha (1-\alpha)^2}{t_\infty} \tag{7}$$

The specific mass transfer rate is computed as $\dot{m} = \dot{m}^+ - \dot{m}^-$. Here, $\bar{p}$ is the filtered pressure, p_v the vaporization pressure and C^+ and C^- empirical constants determining the mass transfer rate. Thus, vaporization occurs when the pressure is below the vapor pressure and there exists some liquid to vaporize, while condensation is restricted to the interface region of the cavity, independent of the pressure, with a maximum at α=1/3 and going to zero in the pure vapor region and the pure liquid region [27].

The Kunz model is not the only available model but has the numerical advantage of having the condensation source/sink term independent from the pressure p. Furthermore, the authors have tested in a previous research [31] that the most widely diffused Sauer model [32], considered more realistic from some authors [33], produces negligible differences in terms of results and imply longer computational times. For this reason, the Kunz model was selected.

While the introduction of the cavitation model extends the applicability of this approach to any "windage" condition (also involving liquids), when two different fluids are present (typically air & lubricant), the approach should be modified again and α assumes the meaning of volume fraction between the two fluids instead the two phases of the same fluid. At the same time, the source term for the phase change is set to zero. In this manner, it is also possible to model the churning condition that takes place in the majority of the real applications.

Three different numerical models were implemented for the study of windage without and with cavitation and for churning phenomena.

4. Spatial discretization

Gear simulations are intrinsically non-stationary. This consideration implies the need to rotate the boundaries corresponding to the teeth flanks. In gearboxes, the topology of the domain is significantly time dependent. As consequence, the mesh that is created for a specific time step will distort with the progress of the calculation loosing quality and leading to numerical instability of the solution. In further steps, the elements will collapse and the simulation cannot proceed anymore. For this reason, it is necessary to adopt some specific mesh handling/regeneration techniques in order to "refresh" the mesh after each or few time steps.

Commercial software make available some specific feature that erase the distorted elements and substitute them with a new tetrahedral grid patch [12,14–16] (Fig. 2b). This approach is effective but not efficient. The new elements result not regularly distributed and often very small in comparison to the initial mesh size. This implies an explosion of the computational effort. Another possible mesh handling strategy is to use an RBM mesh-morphing algorithm as shown by Biancolini [34] for a F1 wing. This approach is very powerful but applicable only for small deformations and, therefore, not to meshing gears. Qi et al. [35] applied an improved form of such method to a gear pump. The algorithm handles the large mesh deformations effectively and enables to hold the same mesh for a complete gear rotation. This approach is extremely efficient in terms of computational time but intrinsically implies to have distorted elements (Fig. 2e). The main goal of simulating a gear pump is to predict the suction and delivery pressures. A distorted mesh generates numerical errors near the boundary of the gears that can be neglected for that purposes. This is not possible if the goal is the determination of pressures and shear stresses on the boundaries themselves and the relative power loss that generates. For this reason, the authors maintain that all these approaches are not adequate for the purposes of this research and have developed a new methodology. Instead of

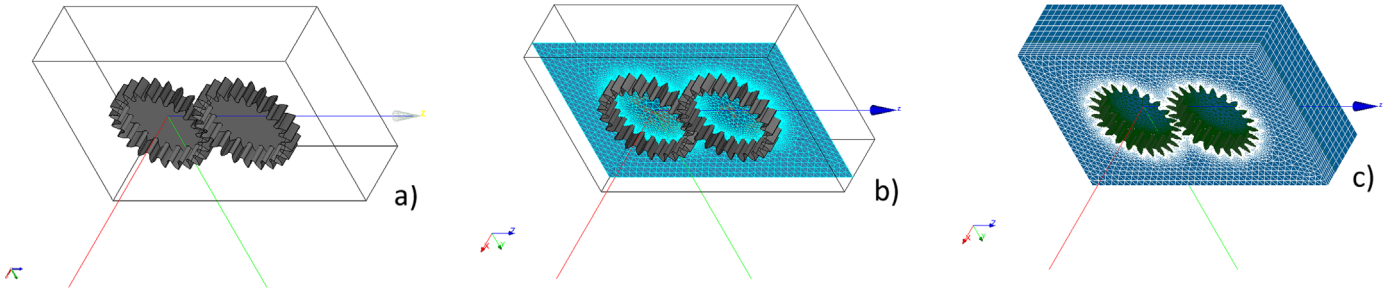

Fig. 1. Mesh generation steps: (a) analytical geometry; (b) mid-plane meshing; and (c) final extruded mesh.

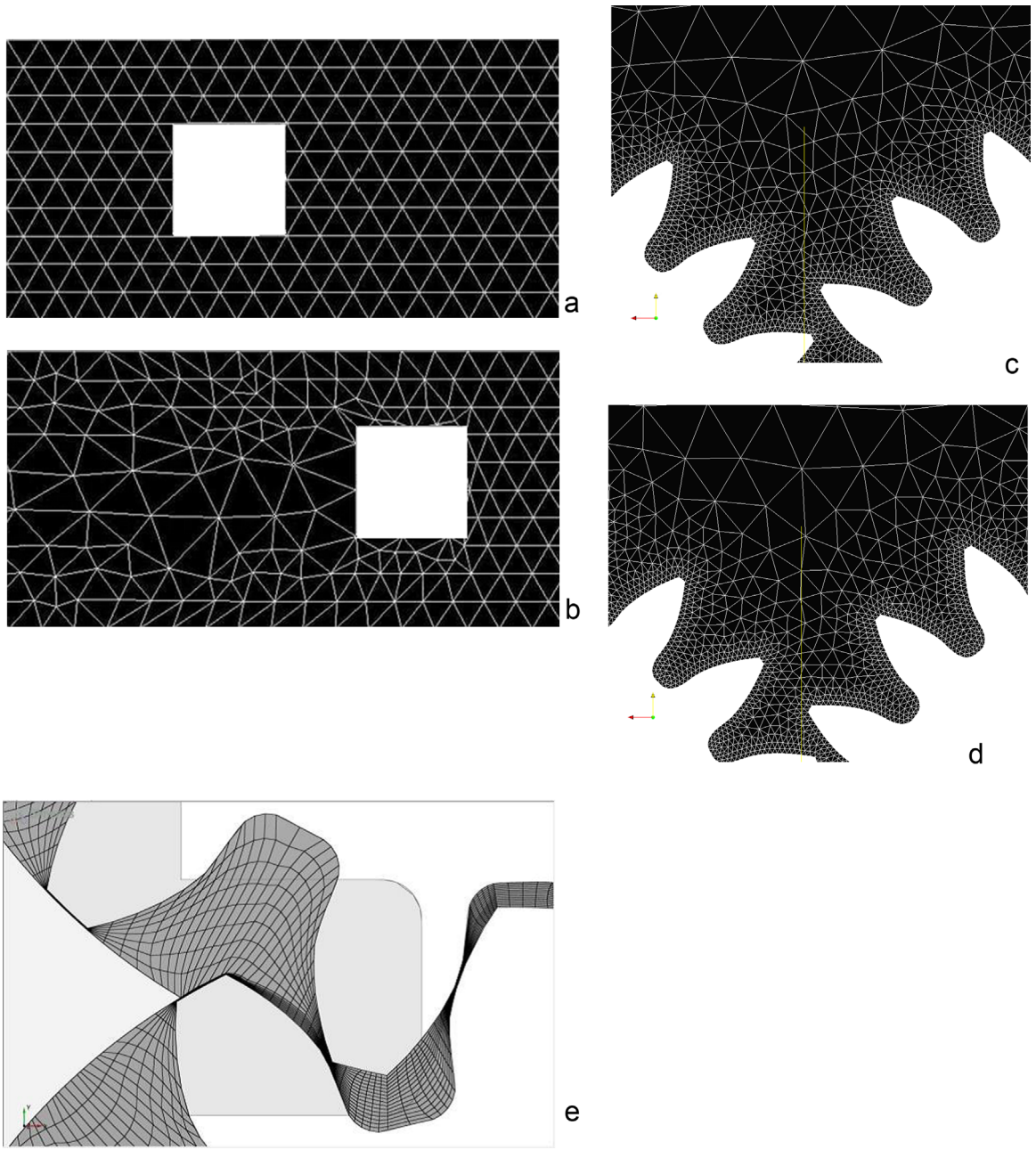

Fig. 2. (a,b) local-based grid-regeneration in a commercial environment; (c,d) grid-substitution-based remeshing with the present approach; and (e) mesh morphing [35].

deforming excessively the elements (mesh morphing) and/or removing just the elements with bad quality (local mesh update), the total mesh is substituted with a new one after a small prescribed deformation. The fields are mapped from the old mesh to the new one. This approach can introduce benefits only if the generation of the new mesh is efficient.

This goal was achieved with the implementation of a special algorithm that analytical handles the geometry and mesh generation [23]. Starting from the main gear parameters such as normal module, number of teeth, addendum and dedendum coefficients as well as shift coefficient, the algorithm generates in few seconds the geometry. The geometry is successively partitioned with parallel planes. The internal planar faces are discretized with a top down strategy that starts by computing the corner points, discretizing the edges and the faces with an advancing front surface mesh generator. A fast Delaunay algorithm generates the mesh. Eventually it fails for the last elements, back-tracking rule-base algorithm takes over [36,37]. Starting from this internal 2D meshes, the 3D mesh is obtained by extruding the planar elements of the 2D partitions corresponding to the gear flanks in one direction and the remaining partition in both directions. This approach is very efficient and allows a drastical reduction the computational effort for the mesh generation.

The mesh density was chosen after a grid independence analysis (mesh from 10 k up to 2 M cells) in order to find the best compromise between quality of the results and computational effort. The geometry used for the model validation consists in 0.5 M cells. The mesh generation (for a single position) on a 12.8 GFLOPS workstation takes approximatively 30 s. The same geometry was previously simulated with a general-purpose commercial software: the initial mesh generation (mesh based on a 2.5-dimensional meshing technique with the same size) takes approximatively 6min [12].

For completeness, another technique should by cited. It is the so-called overlapping grid technique. This approach does not

require any remeshing but suffer from loss of conservation and has local reduced accuracy due to drastic grid size variation resulting inappropriate for the goals of such research.

5. Automatic procedure

The solution flowchart starts reading all the simulation parameters from an input file. All the dictionary templates that control the geometry and mesh generation are updated with the provided parameters. At this point the first mesh is generated, the conservation equations are solved for a prescribed number of time steps according to the allowable mesh deformation that can be handled by the implemented Laplace smoothing equation and the fields stored. The dictionaries are updated and a new mesh is generated for the current angular position of the gears at the considered time step. The previously stored fields are mapped onto the new mesh and the simulation restarts. This until the target simulation-time T_{END} is reached. At this point the velocity, pressure and volume fraction fields are post-processed and the power loss stored into an output file.

6. Model validation

The presented approach was tested on a configuration for which experimental results are available [24]. It consists in a no-load FZG test rig with dip lubrication. The gears are immersed into the oil partially or completely. The gearbox can be filled and closed completely and the oil can be pressurized up to 8 bar. The torque loss of one spur gear set can be measured by a torque meter on the input shaft. Specific tests without the gears enable the characterization of the losses of the bearings. In this manner, the gear loss contribution can be separated from the total measured losses.

Systematic investigations by Otto [38] on an FZG no-load test rig with dip lubrication showed a significant increase of the gear no-load losses in the case of high and highest oil levels. The main effect on the gear no-load power losses of dip-lubricated transmissions is the oil level. Höhn et al. report [24] the no-load torque loss for three operating conditions: partial lubricant filling up to the axis of the gears (50%), complete filling (100% – 1 bar) and complete filling and pressurization (100% – 6 bar). The case with imposed pressurization was adopted on the basis of the observation that with the complete filling at natural pressure, due the oil drag of the gears, they actually resulted only partially immersed during the operation.

7. Results and discussion

Fig. 4 shows a comparison between the experimentally measured results (lines) and the numerical predictions (filled symbols). The three curves represent the complete filling and pressurized condition (100% – 6 bar), the complete filling condition at ambient pressure (100% – 1 bar) and the partial filling (50%) condition respectively. Such conditions were simulated with the three above presented models. One of the objectives of the simulation was also to better understand from the physical point of view what Höhn et al. observed from the phenomenological point of view.

As previously mentioned, Höhn et al. applied an overpressure in order to avoid partial gear immersion due to the effects of the drag of the gears stating that only in this manner the gears are running also during operation completely immersed into the oil. However, as far as the lubricant can be considered as incompressible [30], the two conditions of complete filling at ambient pressure and 6 bar are equivalent in terms of power losses if cavitation does not take place. The applied pressure is hydrostatic and does not affect the resistant torque.

Only the relative pressure variation during operation generates resistance due to its unbalance. The lower resistant torque observed at ambient temperature is, in the opinion of the authors,

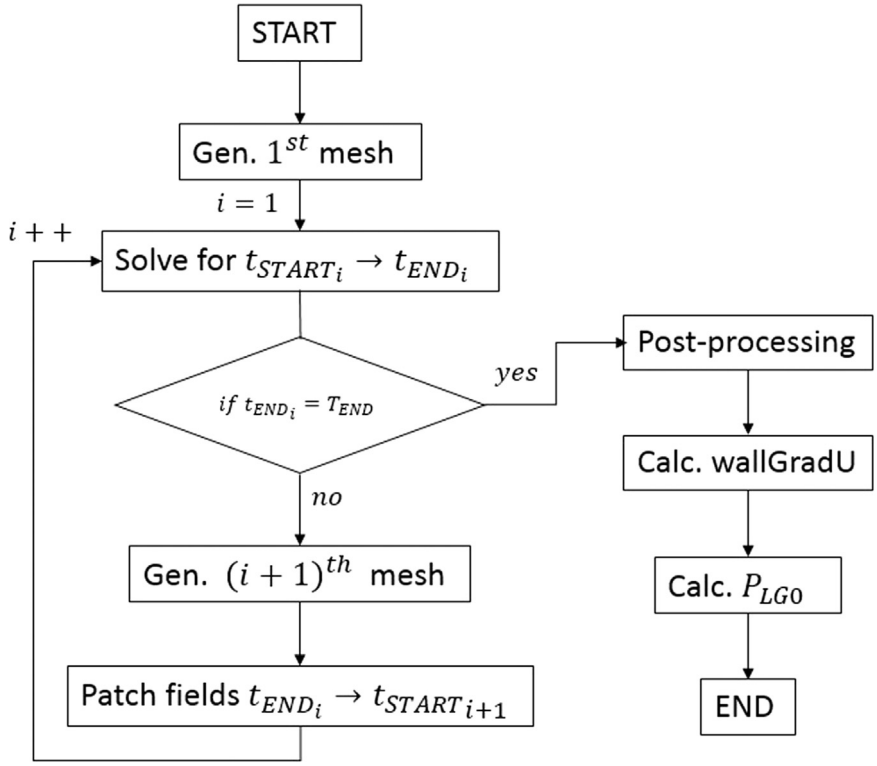

Fig. 3. Automatic procedure flowchart.

not due to the presence of air that surrounds the gear due to the drag of the gear itself as stated in [24] but due to cavitation. Considering that the volume is closed and sealed, once it is filled, no air or only a very small quantity that should not affect the measurements is present inside the gearbox.

When the pressure reaches the vaporization value due to the rotation of the gears, the lubricant changes its state from liquid to vapor. Consequently, there is an intrinsic compensation of negative pressures that cannot decrease under p_v. When cavitation is neglected, both positive and negative (relative) pressures can grow without limits in their magnitude and contribute to the resistant torque. By admitting cavitation, the minimum value of the pressure is limited by the vaporization pressure so the contribution in terms of resistant torque is mainly due to the overpressures (absolute value of a higher order of magnitude with respect to the negative pressures). Considering that positive and negative pressures generate on opposite flanks, it appears that both give a positive contribution to the resistant torque. A limitation of the negative permissible value for the pressure implies a limitation of the contribution to the power loss phenomenon. This consideration is supported by the numerical predictions that agree with the experimental measurements also for the not pressurized condition. This implies that, in such condition, the gears are, despite of what reported in [24], surrounded by oil only (in both its states).

Fig. 5 shows the volume fraction and the pressure distribution for the ambient pressure operating conditions and for a tangential speed of 38 m/s. The rear flank of each tooth is cavitating and the pressure results limited by the vaporization pressure. This phenomenon appears obvious by looking at the volume fraction contour. In the closing gap, the pressure is significantly increased and only liquid phase is present. Furthermore, a pressure gradient in the axial direction is visible, confirming that the pocketing/squeezing phenomenon occurs. In the opening gap the pressure is below the ambient pressure and cavitation takes place on the whole tooth high except for the line of contact where a film layer prevents the direct contact of the flanks (highlighted in Fig. 5a).

Fig. 6 shows the completely different velocity fields that develop with and without considering cavitation. While no cavitation is present, a fluid wake generates near the start of the contact. Cavitation prevents the wake formation. In the vane between two gears, the velocity field is very different. While the lubricant is not cavitating, the velocity profile is more or less symmetric except for the pressure peak at the top of the teeth, while when vapor is present, the velocity sink drastically in the caviting region.

The results obtained in the pressurized condition are comparable with the findings of other authors [40] in terms of pressure distribution. On the other side, no results are available in literature concerning cavitation in gearboxes except for the contribution given

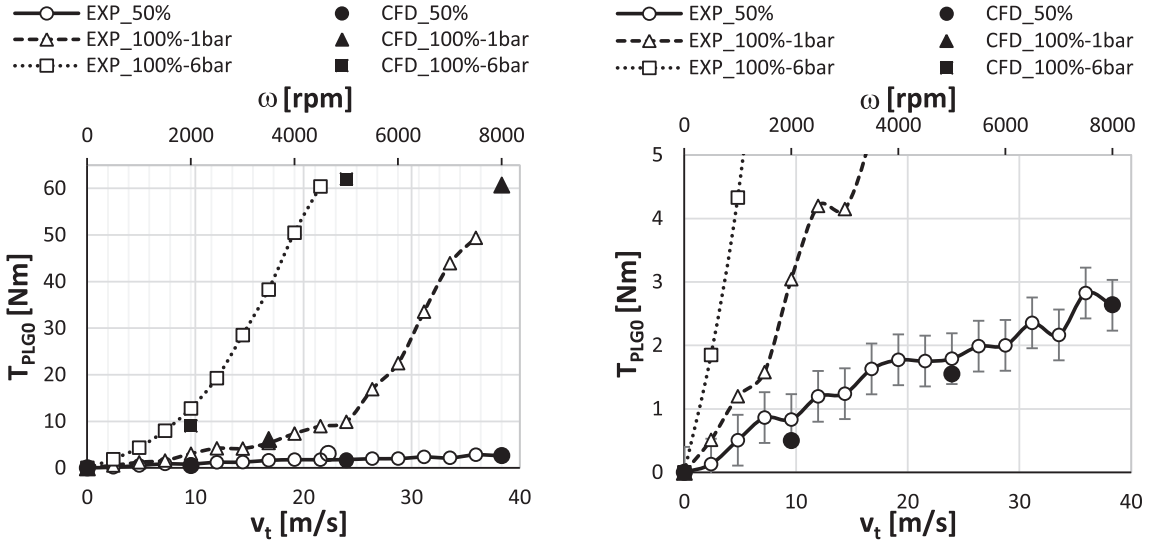

Fig. 4. Comparison between the numerical and the experimental results.

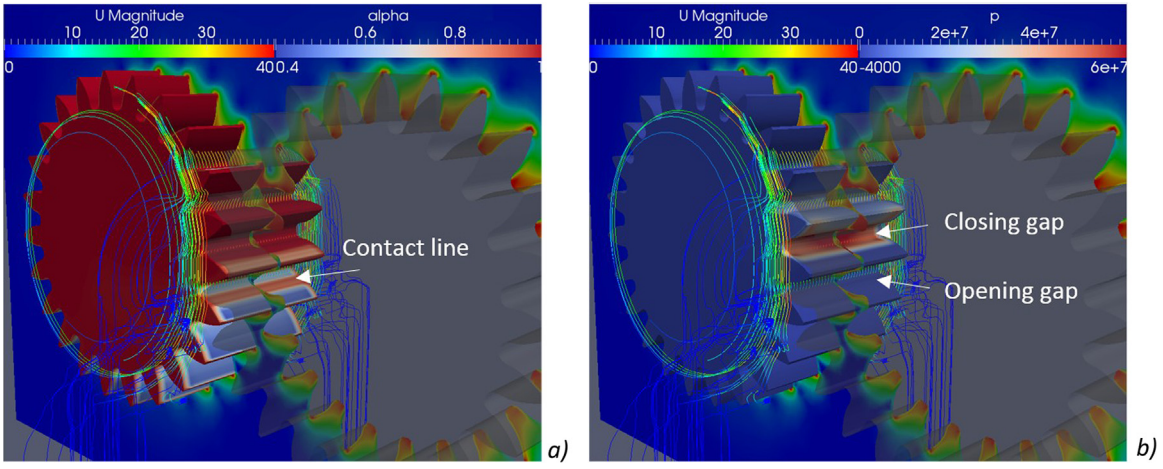

Fig. 5. 100% – 1 bar – 38 m/s: velocity contour on the symmetry plane [m/s]: (a) volume fraction of the liquid phase on the gear [ ] and (b) pressure on the gear [Pa].

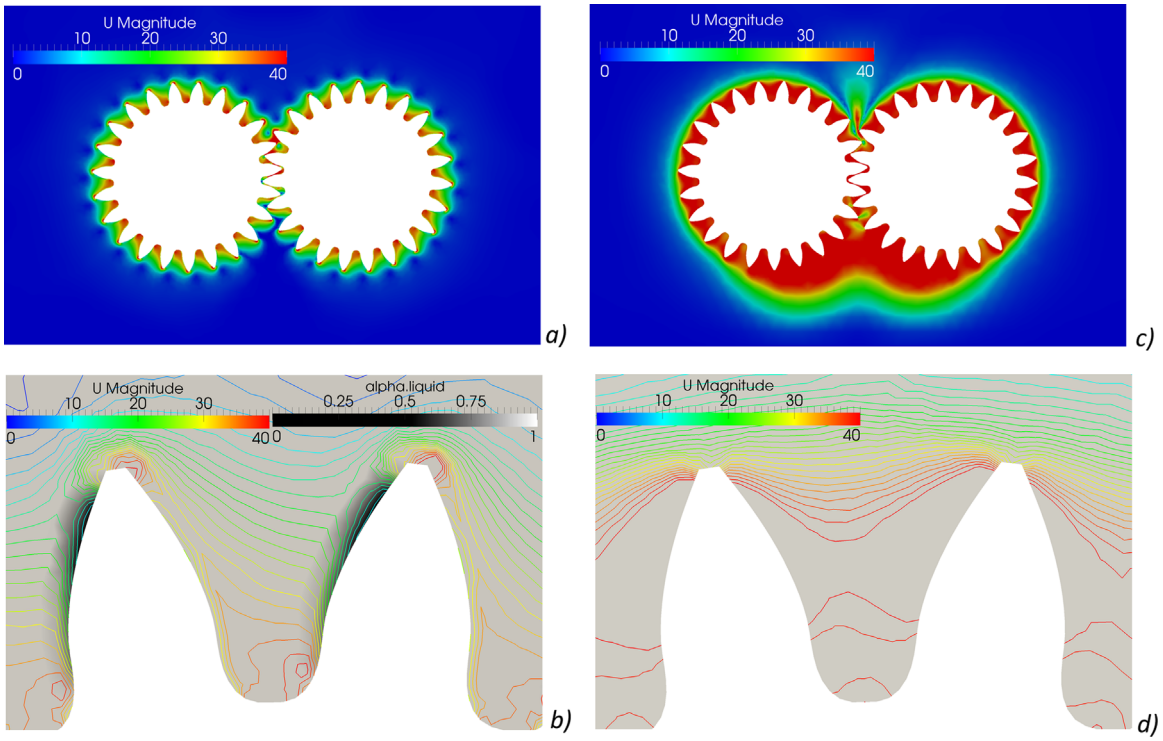

Fig. 6. 38 m/s: velocity contour and volume fraction contour on the symmetry plane [m/s]: (a,b) 100% – 1 bar; (c,d) 100% – 6 bar.

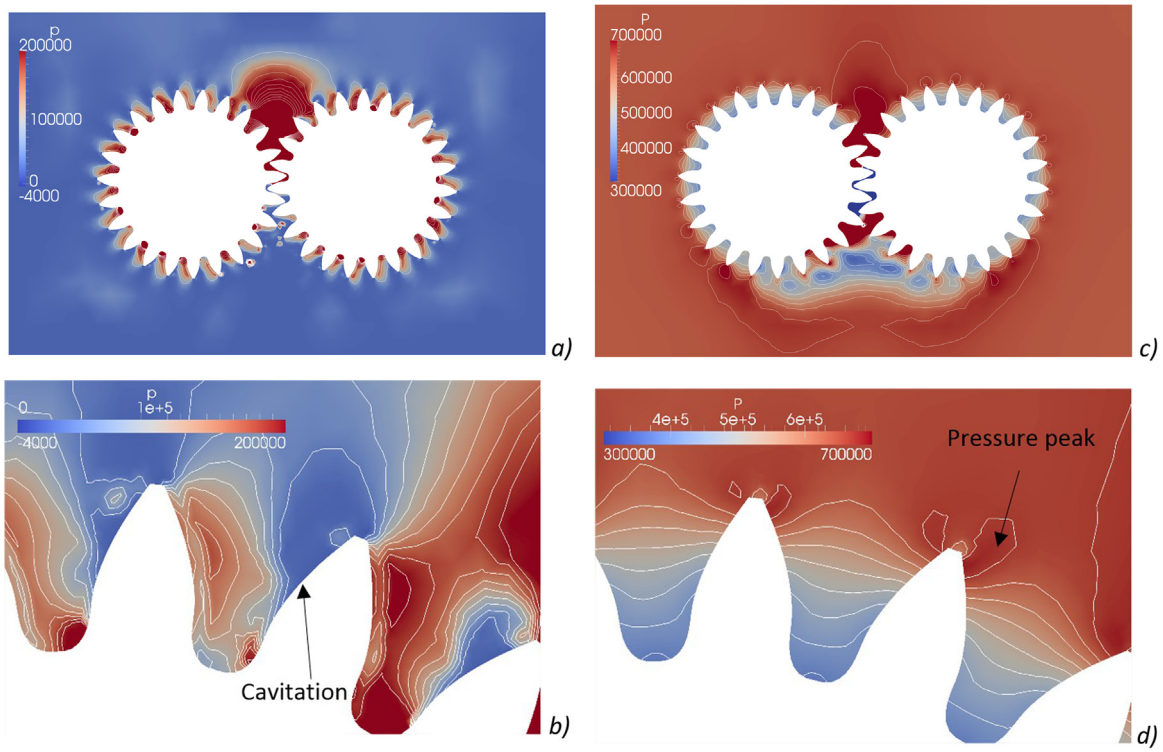

Fig. 7. 38 m/s: pressure contour on the symmetry plane [Pa]: (a,b) 100% – 1 bar; (c,d) 100% – 6 bar.

by Hunt et al. [41]. Fig. 7a shows a relevant pressure decrease in the upper part of the rear flank of the gear down to the vaporization pressure. This causes an unsymmetrical pressure field inside the vane between two teeth. Meanwhile, the front flank does not shows the pressure peak on the top corner that is typical of windage.

Fig. 8 shows the different trajectories of the fluid particles. While in the pressurized condition the lubricant that leaves axially the vane is sucked in the next vanes by the lower pressures, in the non-pressurized condition, the cavitation phenomenon limits the lower value of pressure and the gradient is not enough to suck the lubricant expelled axially from one vane in the next one. Consequently, eddies generates as shown in Fig. 8c.

Finally, a partially filled condition was simulated. The presence of air reduces drastically the resistant torque. Fig. 9 shows the evolution of the air-oil interface.

Fig. 10 reports the volume fraction and velocity fields. It

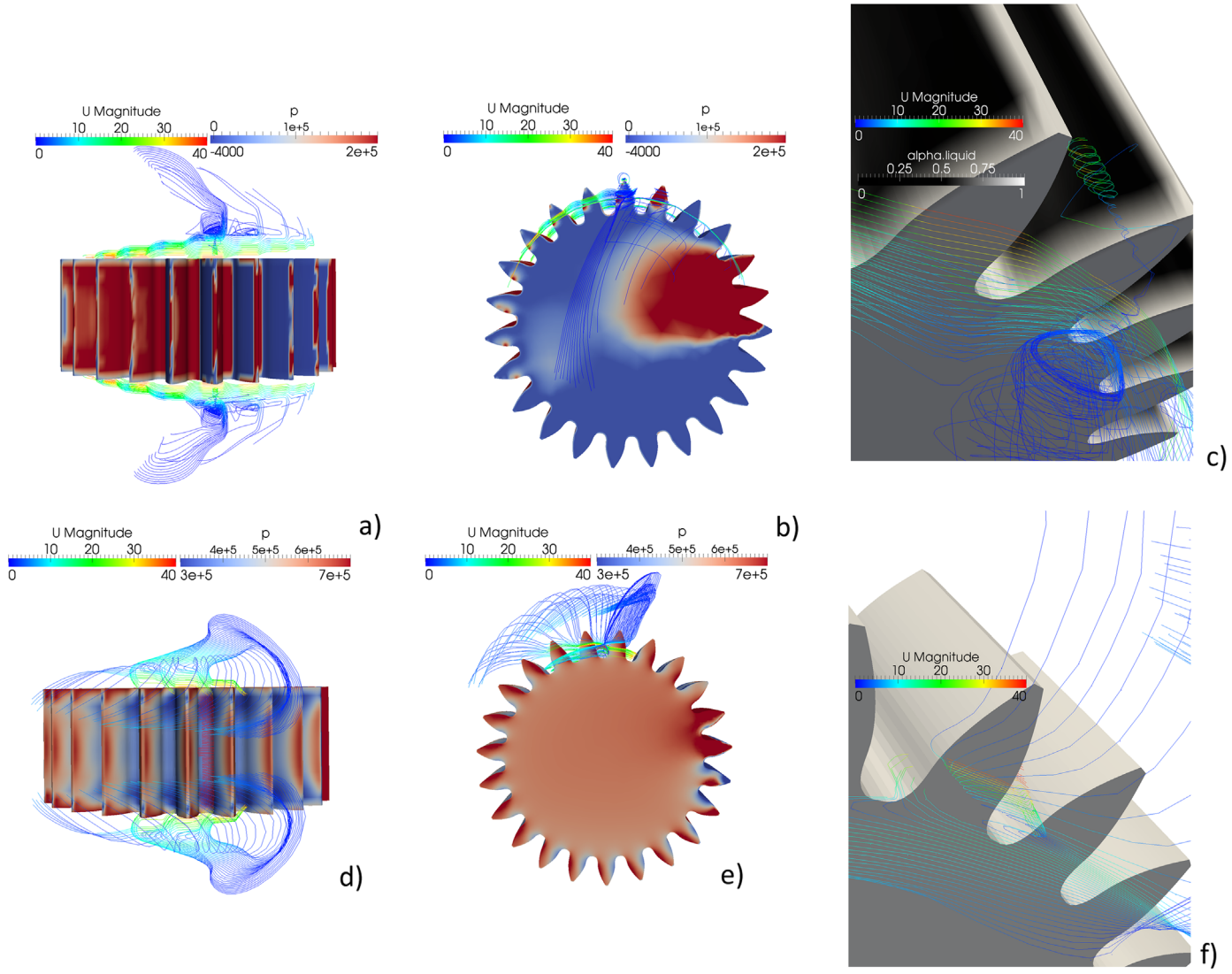

Fig. 8. 38 m/s: (a–c) 100% – 1 bar (cavitation present); (d–f) 100% – 6 bar (pressurized, no cavitation) – Pathlines colored according to the U Magnitude [m/s], gear flanks colored according to the p [Pa] or (c) to the volume fraction.

appears clearly that the velocity is higher where the lubricant volume fraction is lower. This due to the different viscosities and densities of the two fluids. In the vane between the teeth that lie in the oil bath, air pillows generate after few rotations confirming the findings of Chernoray's experiments [42]. The prevalence of the inertial contribution over the viscous one leads to thin boundary layers and a confined region of induced flow very close to the wheel.

Under the engagement, a significant amount of air is trapped in the oil bath, evidence confirmed by other authors [43].

In the upper part of the gearbox, an oil stream generates from the teeth that leave the bath. The streams can break-up and lead to formation of droplets. From each tooth that exits the bath, small lubricant rivulets leave the gear radially (Fig. 11a): most of the oil is hurled off the teeth by the centrifugal force before they engage again ad shown also by Otto [44]. The simulations show that the main stream leaves the gears after approximately 270° (detachment-angle) starting from the engagement confirming the findings of Otto [44]. For high rotational speeds, the oil stream reaches the walls of the housing and plunges in the oil bath again agitating the free surface and generating bubbles in the oil.

8. Performance enhancements

The computational effort needed for the above presented windage simulation with the new procedure the flowchart of which is described in the Automated Procedure chapter was compared to the effort needed to simulate the same geometry with a commercial code. The simulations took approximately 20 h on 16 3.3 GHz CPUs (211 GFLOPS) with the tested general-purpose commercial software [12] and just 21 h on a single 3.2 GHz CPU (12.8 GFLOPS) to reach the regime condition (approximately 3 rotations of the gears) with a net reduction of the computational time of 93.5% (considering a perfect scalability [45]). The simulation time is sheared between the different steps in this manner: simulations of 25 time steps (with $Co < 0.3$) (84.8%), generation of the new mesh (12.7%), mapping of the results (2.5%). The time reduction showed by the new approach is due to a better meshing efficiency that has both a direct positive impact on the meshing computational time and on the numerical simulation time. Due to a more regular mesh, in fact, the solver can perform the calculation in a reduced number of time steps without losing stability ($Co < 0.3$) contributing to a further reduction of the computational effort.

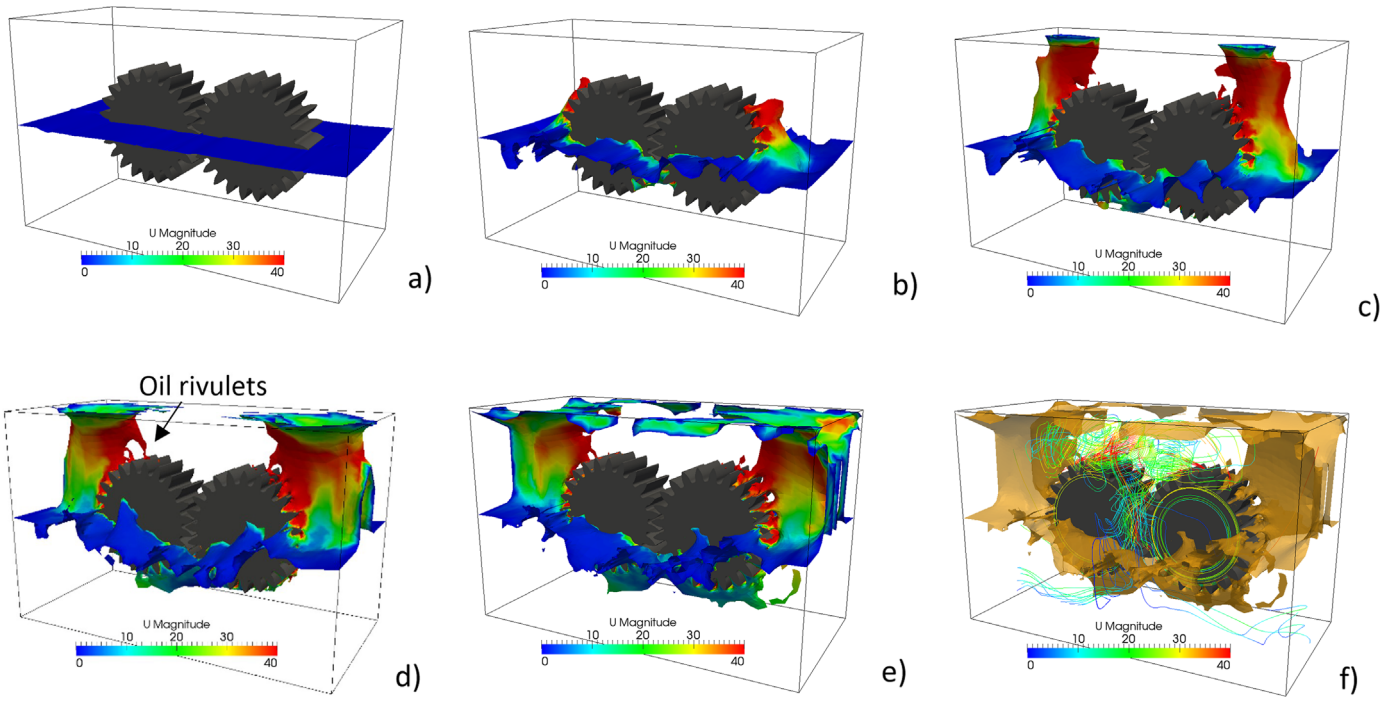

Fig. 9. 50% – 38 m/s: (a–e) evolution of the phase interface; and (f) pathlines.

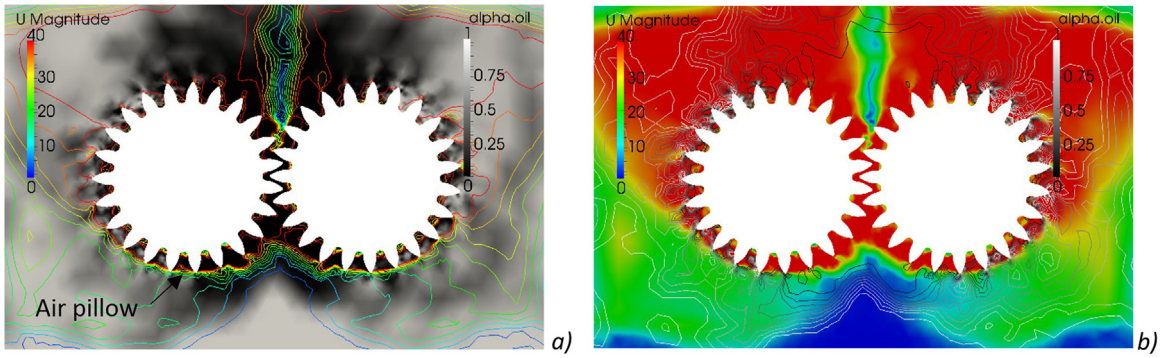

Fig. 10. 50% – 38 m/s: (a) volume fraction contour on the symmetry plane (U Magnitude isolines [m/s]); and (b) velocity contour on the symmetry plane [m/s] (volume fraction isolines [ ]).

9. Conclusions

The study of the lubricant fluxes and the related power losses inside a gearbox is traditionally based on experimental evidences. Recently some research was carried out with commercial simulation software. In this study, a gear-specific simulation tool was developed. The kernel of the code relies on three separate solvers in order to model all the main phenomena that can take place in gearboxes; windage, churning and cavitation.

The presented numerical approach introduce undoubted benefits in terms of computational effort (− 93.5%) with respect to the state of the art in terms of general-purpose simulation software for such purposes. This is primarily due to a more effective mesh-handling algorithm.

The model was applied to a geometry for which experimental results were available. The comparison was made in terms of resistant torque for different rotational speeds, filling levels and operating pressures showing a good agreement.

The results of the simulation for the complete oil filling conditions have shown the important role of the vaporization pressure of the lubricant in the phenomenon of power dissipation. Once the local pressure reaches the vaporization pressure, the lubricant changes its state from liquid to vapor preventing a further pressure decrease. The phase change modifies also significantly the oil patterns and the velocity profiles. This pressure and velocity fields modifications have a huge impact on the resistant torque that results reduced by a factor 5-6 with respect to the pressurized and not caviting condition. It is worthy to point out that, without taking into account properly the phenomenon of the cavitation, it could not possible to explain with the CFD simulation the different behavior of the two cases with the complete filling of the housing with a liquid lubricant, respectively at natural pressure or with overpressure.

Considering the partial oil filling, the results of the simulations were compared with data available in literature not only in terms of resistant torque but also in terms of lubricant distribution.

The resistant torque predictions have proved to be very accurate. The comparison of the numerical results with high-speed-cameras pictures from different authors show that the developed approach is capable to well predict also other aspects like, for example, the lubricant detachment-angle of 270°, the formation of air pillows and the air trapping phenomenon. The powerful capabilities of this approach make it a potential tool for an advanced design of gearboxes as well as a powerful tool for a further comprehension of the physics behind the gearbox lubrication.

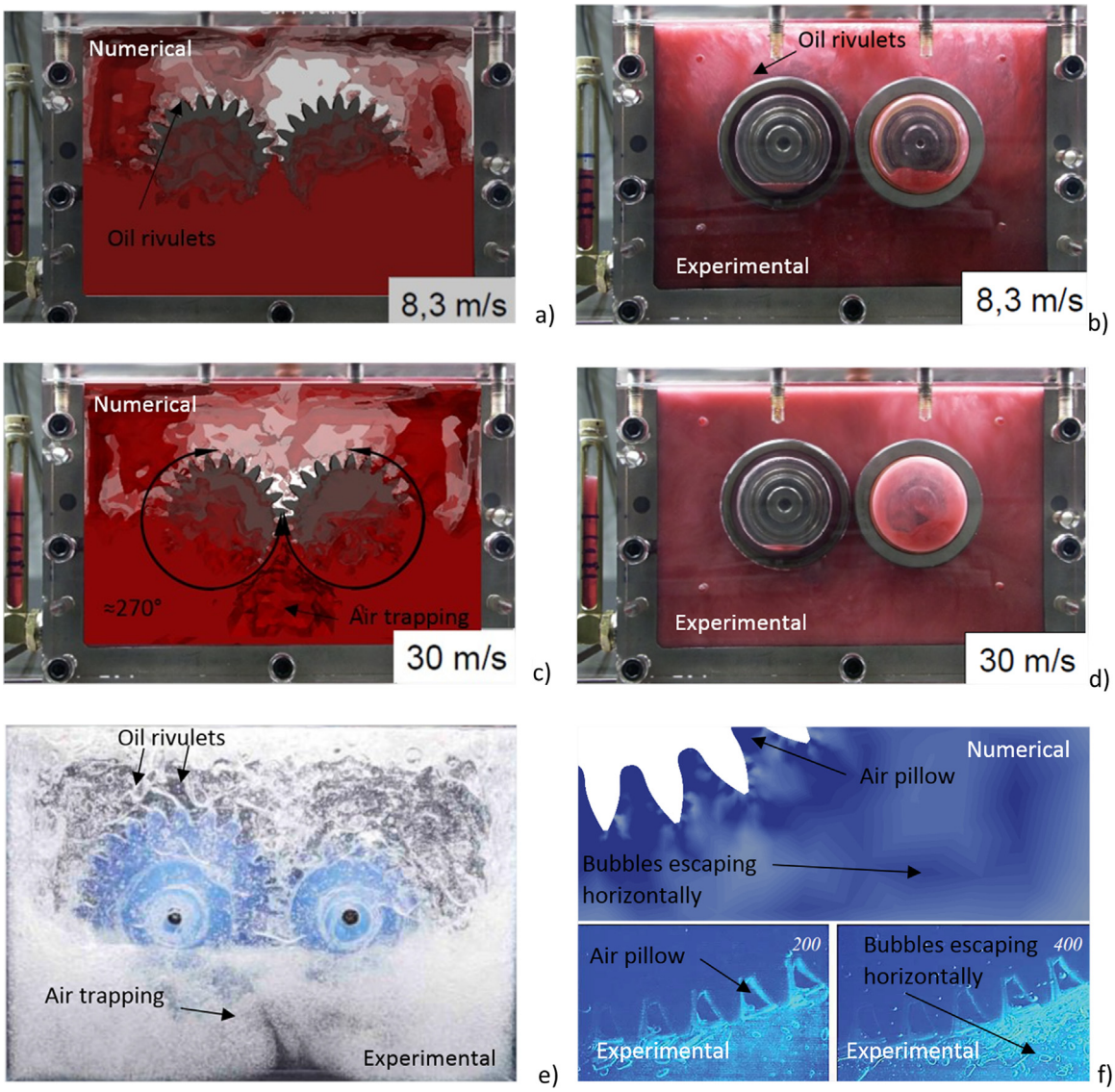

Fig. 11. (a) Numerical results for a tangential speed of 8.3 m/s; (b) experimental [38] results for a tangential speed of 8.3 m/s; (c) numerical results for a tangential speed of 30 m/s; (d) experimental [38] results for a tangential speed of 30 m/s; (e) experimental observation of the fluid distribution according to [43]; and (f) air pillows formation: experimental evidence according to [42] (below) and numerical results of present study (above).

References

[1] Daily J, Nece R. Chamber dimension effects of induced flow and frictional re-sistance of enclosed rotating disks. ASME J Basic Eng 1960;82:217–32.

[2] Mann R, Marston C. Friction drag on bladed disks in housings as a function of reynolds number, axial and radial clearance, and blade aspect ratio and solidity. ASME J Basic Eng 1961;83:719–23.

[3] Soo SL, Princeton NJ. Laminar flow over an enclosed rotating disk. Trans ASME 1958;80:287–96.

[4] Terekhov AS. Hydraulic losses in gearboxes with oil immersion. Vestnik Mashinostroeniya 1975;55:13–7.

[5] Lauster E, Boos M. Zum Wärmehaushalt mechanischer Schaltgetriebe fьr Nutzfahrzeuge. VDI-Ber 1983;488:45–55.

[6] Boness RJ. Churning losses of discs and gears running partially submerged in oil. In: Proceedings of the ASME international power transmission gearing conference, vol. 1. Chicago; 1989. p. 355–9.

[7] Changenet C, Velex P. A model for the prediction of churning losses in geared transmissions – preliminary results. ASME J Mech Des 2007;129(1):128–33.

[8] Walter P, Langenbeck K. Anwendungegrenzen für die Tauchschmierung von Zahnradgetrieben. Plansch- und Quetschverluste bei Tauchschmierung 1982 Frankfurt/M: Antriebstechnik.

[9] Mauz W. Hydraulische Verluste von Strinradgetrieben bei Umfansgsgeschwindigkeiten bis 60 m/s.Stuttgart: IMK; 1987.

[10] Marchesse Y, Changenet C, Ville F, Velex P. Investigation on CFD simulations for predicting windage power losses on spur gears. J Mech Des 2011:133.

[11] Hill MJ, Kunz RF, Medvitz RB, Handschuh RF, Long LN, Noack RW, Morris PJ. CFD analysis of gear windage losses: validation and parametric aerodynamic studies. J Fluid Eng 2011;133.

[12] Gorla C, Concli F, Stahl K, Höhn BR, Michaelis K, Schuliteiß H, Stemplinger J- P. Hydraulic losses of gearbox: CFD analysis and experiments. Tribol Int 2013;66:337–44. http://dx.doi.org/10.1016/j.triboint.2013.06.005.

[13] Gorla C, Concli F, Stahl K, Höhn BR, Michaelis K, Schultheiß H, Stemplinger J- P. CFD simulation of splash losses of a gearbox. Adv Tribol 616923, 2012. http://dx.doi.org/10.1155/2012/616923.

[14] Concli F, Gorla C. Analysis of the oil squeezing power losses of a spur gear pair by mean of CFD simulations. In: Proceedings of the ASME 2012 11th Biennial conference on engineering systems design and analysis, ESDA, vol. 2; 2012. p. 177–184, http://dx.doi.org/10.1115/ESDA2012-82591.

[15] Concli F, Gorla C. A CFD analysis of the oil squeezing power losses of a gear pair, computational and experimental study. Int J Comput Methods Exp Meas 2014;2(2):157–67. http://dx.doi.org/10.2495/CMEM-V2-N2-157-167.

[16] Concli F, Gorla C. Oil squeezing power losses in gears: a CFD analysis. WIT Trans Eng Sci 2012;74:37–48. http://dx.doi.org/10.2495/AFM120041.

[17] Gorla C, Concli F, Stahl K, Höhn BR, Michaelis K, Schultheiß H, et al. Load independent power losses of ordinary gears: numerical and experimental analysis. In: Proceedings of the 5th world tribology congress (WTC), vol. 2; 2013. p. 1243–6.

[18] Concli F, Gorla C, Conrado E. Analysis of power losses in an industrial planetary speed reducer: measurements and computational fluid dynamics calculations. Proc Inst Mech Eng Part J: J Eng Tribol 2014;228(1):11–21, http://dx.doi.org/10.1177/1350650113496980.

[19] Concli F, Gorla C. Computational and experimental analysis of the churning power losses in an industrial planetary speed reducer. WIT Trans Eng Sci

2012;74:287–98. http://dx.doi.org/10.2495/AFM120261.
[20] Concli F, Gorla C. Influence of lubricant temperature, lubricant level and rotational speed on the churning power loss in an industrial planetary speed reducer: computational and experimental study. Int J Comput Methods Exp Meas 2013;1(4):353–66. http://dx.doi.org/10.2495/CMEM-V1-N4-353-366.
[21] Concli F, Della Torre A, Gorla C, Montenegro G. Churning power losses of ordinary gears: a new approach based on the internal fluid dynamics simulations. Lubr Sci 2015;27:313–26. http://dx.doi.org/10.1002/ls.1280.
[22] OpenFOAM. ⟨http://www.openfoam.com⟩.
[23] Concli F, Della Torre A, Gorla C, Montenegro G. A new integrated approach for the prediction of the power losses of gears: development of a mesh-handling algorithm to reduce the CFD simulation time. Adv Tribol 2957151, 2016. http: //dx.doi.org/10.1155/2016/2957151.
[24] Höhn B-R, Michaelis K, Otto H-P. Influences on no-load gear losses. Ecotrib 2011;2011(2):639–44.
[25] Strasser D. Einfluss des Zahnflanken- und Zahnkopfspieles auf die Leerlaufverlustleistung von Zahnradgetrieben, Bochum; 2005.
[26] Jakobsson B, Floberg L. The finite journal bearing, considering vaporization (Das Gleitlager von endlicher Breite mit Verdampfung); 1957.
[27] Ubbink O. Numerical prediction of the two fluid systems with sharp interfaces. University of London; 1997.
[28] Rusche H. Computational fluid dynamics of dispersed two-phase flows at high phase fractions [Ph.D. thesis]. London: Department of Mechanical Engineering Imperial College of Science, Technology & Medicine; 2002.
[29] Kunz RF, Boger DA, Stinebring DR, Chyczewski TS, Lindau JW, Gibeling HJ, Venkateswaran S, Govindan TR. A preconditioned Navier–Stokes method for two phase flows with application to cavitation prediction. Comput Fluids 2000;29(8).
[30] Bensow RE, Bark G. Simulating caviting flows with LES in OpenFoam, In: V european conference on computational fluid dynamics ECCOMAS CFD, Lisbon; 2010.
[31] Concli F. Pressure distribution in small hydrodynamic journal bearings considering cavitation: a numerical approach based on the opensource CFD code OpenFOAM®. Lubr Sci 2016. http://dx.doi.org/10.1002/ls.1334.
[32] Sauer J. Instationären kaviterende Sträömung - Ein neues Modell, basierend auf Front Capturing (VoF) and Blasendynamik. Universität Karlsruhe; 2000.
[33] Vaz G, Hally D, Huuva T, Bulten N, Muller P, Becchi P. Cavitating flow calculations for the E779A propeller in open water and behind, In: Fourth international symposium on marine propulsors conditions: code comparison and solution validation. Austin, Texas, USA; 2015.
[34] Biancolini M. Fluid structure interaction with RBF Morph – a generic formula 1 front end. In: Proceedings of the CAE conference. Verona, Italy; 2011.
[35] Qi F, Dhar S, Nichani V, Srinivasan C, Wang D, Yang L, Bing Z, Yang J. A CFD study of an electronic hydraulic power steering helical external gear pump: model development, validation and application. SAE Int 2016. http://dx.doi.org/10.4271/2016-01-1376.
[36] Netgen. ⟨www.hpfem.jku.at/netgen/⟩.
[37] Schöberl J. An advancing front 2D/3D-mesh generator based on abstract rules. Computing and visualization in science. Springer; 1997.
[38] Otto H-P. Flank load carrying capacity and power loss reduction by minimized lubrication. Diss TU München 2009.
[40] Chaari F, Romdhane MB, Baccar W, Fakhfakh T, Haddar M. Windage power loss in spur gear sets. Wseas Trans Appl Theor Mech 2012.
[41] Hunt JB, Ryde-Weller AJ, Ashmead FAH. Cavitation between meshing gear teeth. Wear 1981;71(1):65–78.
[42] Chernoray V, Jahanmiri M. Experimental study of multiphase flow in a model gearbox. Comput Methods Multiphase Flow VI 2011;153.
[43] Andersson M. Churning losses and efficiency in gearboxes [Dissertation]. Stockholm: Royal Institute of Technology; 2014.
[44] Otto H-P. Flank load carrying capacity and power loss reduction by minimised lubrication Dissertation 0166. Technischen Universität München; 2008.
[45] Scalability of ANSYS 16 applications and Hardware selection: on multi-core and floating point accelerator processor systems, ⟨www.ansys.com⟩.